Influence of loading conditions and temperature on static friction and contact ageing of hydrogels with modulated microstructure

Tooba Shoaib†, and Rosa M. Espinosa-Marzal§†*

§ Civil and Environmental Engineering, University of Illinois at Urbana-Champaign, 205 N.
Matthews Avenue, Urbana, Illinois 61801, United States.

†The Materials Science and Engineering, University of Illinois at Urbana-Champaign, 1304 W Green St, Urbana, Illinois 61801, United States.

KEYWORDS. Hydrogels, static friction, contact ageing, biolubrication, colloidal probe atomic force microscopy.

ABSTRACT

Biological tribosystems enable diverse functions of the human body by maintaining extremely low coefficients of friction via hydrogel-like surface layers and a water-based lubricant. While stiction has been proposed as precursor to damage, there is still a lack of knowledge about its origin and the relation to the hydrogels' microstructure, which impairs the design of soft matter as

replacement biomaterials. In this work, the static friction of poly(acrylamide) hydrogels with modulated composition was investigated by colloidal probe lateral force microscopy as a function of load, temperature and loading time. Temperature-dependent studies enable to build a phase diagram for hydrogel's static friction, which explains stiction via (polymer) viscoelastic and poroelastic relaxation, and a subtle transition from solid- to liquid-like interfacial behavior. At room temperature, the static friction increases with loading time, a phenomenon called contact ageing, which stems from the adhesion of the polymer to the colloid and from the drainage-induced increase in contact area. Contact ageing is shown to gradually vanish with increase in temperature, but this behavior strongly depends on the hydrogel's composition. This work scrutinizes the relation between microstructure of hydrogel-like soft matter and interfacial behavior, with implications for diverse areas of inquiry, not only in biolubrication and biomedical applications, but also in soft robotics and micro-electromechanical devices, where the processes occurring at the migrating hydrogel interface are of relevance. The results support that modulating the hydrogel's mesh size and the near-surface region is a means to control static friction and adhesion. This conceptual framework for static friction will foster further understanding of the wear of hydrogel-like materials.

1. INTRODUCTION

When two surfaces are in contact and move relative to each other, friction occurs at the interface. Biological tribosystems, like respiratory and gastrointestinal tracts, oral cavity, articular cartilage and corneal epithelium, enable diverse functions of the human body by maintaining extremely low coefficients of friction possibly life-long. The exceptional lubrication behavior of biological tribosystems stems from their common composition, a macromolecular network with a water-based lubricant. For example, articular cartilage is a complex avascular tissue composed of an

extracellular matrix of collagen II and proteoglycans with a well-ordered three-dimensional structure, a small number of embedded chondrocytes cells and ~70%-80% interstitial fluid. Articular loading has been reported to play a key role in facilitating the biphasic lubrication of the tissue, contributing to the tissue's low coefficient of friction, and stimulating chondrocyte metabolism and mechanotransduction.²⁻⁵ Several works agree in that a much softer amorphous (gel) layer of tens of microns in thickness covers the cartilage and holds even larger amounts of water.⁶⁻⁷ This gel-like surface layer is very soft (elastic modulus ~9 kPa) and is composed of proteoglycans along with gel-forming mucins and phospholipids. ⁶⁻¹⁰ It has been proposed that this superficial gel layer helps to maintain a low friction coefficient during boundary lubrication.⁶

Due to its avascular nature, articular cartilage has a poor self-healing ability, thus, posing a challenge for joint recovery. Thus, one of the key pending questions concerns the origins and prevention of cartilage damage. Several works have showed that prolonged static (non-sliding) loading leads to the squeeze-out of the fluid from the superficial zone, 11-12 and thereby to an increase in adhesion and friction, 12 which has been related to joint fatigue and wear of the cartilage's surface. Turthermore, damage of the cartilage's surface was not found to be directly related to dynamic friction, but instead, to the static friction before sliding commences (i.e. stiction). Stiction happens when the adhesion between the contacting bodies is so high that it prevents interfacial motion. Insight into the mechanisms underlying stiction is, however, still lacking. This hinders understanding and prevention of wear as well as the design of replacement materials with sufficient strength and toughness and concomitant lubricity and wear resistance. 15

In the context of dry friction, experimental studies have shown an increase in static friction with the increase of loading time, a phenomenon commonly known as contact ageing. Adhesion models lie give the static friction as the critical shear strength of the interface at the commencement of

motion (σ_s) multiplied by the true contact area (A_r). Contact ageing has been majorly related to the increase in the true contact area with time due to plastic or viscoelastic creep of multi-asperity contacts. Strengthening due to chemical bonding across the interface, e.g. for polymers glasses¹⁶, is considered a concomitant process that contributes to contact ageing through the increase in interfacial shear strength. If contact ageing occurs, as per its thermally activated origin, the static friction is observed to increase logarithmically with loading time. However, deviations from a logarithmic relation between static friction and loading time have been often reported.¹⁷⁻¹⁹

Because of their structural and compositional semblance to biological tribosystems, synthetic hydrogels, which are biphasic materials composed of a polymer network and large amounts of water, are physiologically relevant model systems, both to investigate biologically mediated lubrication ²⁰ and as materials for replacement and regeneration of biological tissues, ²¹⁻²² including cartilage.²³ The analogy in behavior has been also proved by theory, e.g. in the context of the interaction between colonic mucus hydrogels and (gut) polymers, which follows classical polymer theory.²⁴ Based on just a handful of precedent studies,²⁵⁻²⁹ the same two mechanisms have been proposed to be responsible for hydrogel's static friction. For instance, Baumberger et al. proposed that the increase in static friction at gelatin/glass interfaces with hold time stems from the reconfiguration of confined polymer chains, which gradually pin to the glass countersurface.²⁶ However, this argument alone could not explain the different extent of contact ageing of the investigated hydrogels. Based on confocal microscopy images, it was proposed later that, when the interfacial water between (agar) hydrogel and a glass surface is squeezed-out under static loading, more multiple contact junctions form gradually with time within the apparent contact area.²⁷ A logarithmic increase of static friction with hold time was reported for poly(Nisopropylacrylamide) hydrogels.²⁹ A more complex picture emerged from a study of the effect of temperature on the static friction between like-charged hydrogels.²⁸ Here, the static friction was shown to decrease with temperature, and a maximum, not discussed by the authors, emerged at low temperature. The origin of this behavior was loosely attributed to the influence of temperature on the structure of hydration water. While this argument is difficult to rationalize in our opinion, their experimental finding suggests that the mechanisms underlying hydrogel's static friction are actually more intricate than originally proposed.

Here, we have investigated the effect of load, sliding velocity, temperature and contact time on static friction and adhesion between polyacrylamide (PAAm) hydrogels with three different compositions and a silica colloid using Atomic Force Microscopy (AFM). PAAm hydrogels not only afford control of the mesh size of the polymer network, but their hydrophilicity, microstructure and mechanical behavior resembles that of cartilage's surface layer. Current replacement materials for cartilage still lack perfection due to inadequate lubrication, wear, as well as the induced weakening of the surrounding tissue and protein denaturation. Control of static friction is crucial for optimal design of replacement materials because of its recognized relation to cartilage wear. Our experimental study answers this call to advance knowledge and reveals a phase diagram for the static friction of hydrogel-like materials as well as the influence of hydrogel's microstructure; its implications for biological tribosystems are also discussed.

2. EXPERIMENTAL METHODS

2.1 Hydrogel preparation. All experiments were conducted on PAAm hydrogels. Acrylamide 40% w/v solution (monomer), N.N'-methylene bis(acrylamide) (crosslinker), ammonium persulfate (initiator) and tetramethylethylenediamine (TEMED) (accelerator) were purchased from Sigma-Aldrich (USA). PAAm hydrogels were prepared with 4, 5 and 8 wt% of the acrylamide monomer in DI water and 0.1, 0.30 and 0.48 wt% of bisacrylamide, respectively, and are referred

to as 4%, 6% and 9% hydrogels in the following; in our previous works, 9% hydrogels were called 12% hydrogels.³¹⁻³² Each solution was degassed for 15 minutes prior to the addition of 1/100 and 1/1000 of the initiator and the accelerator, respectively. After this, 800 μL of the solution was quickly pipetted onto a hydrophobic glass slide and the droplet was covered with a hydrophilic coverslip. Gelation of the sandwiched solution was allowed to proceed for 30 minutes, after which the coverslip with the hydrogel was removed from the hydrophobic glass slide and rinsed in DI water to remove any excess of solution. The final thickness of the hydrogels was ~2 mm. The hydrogel samples were stored in DI water at 4 °C for one day prior to any testing. All measurements were done on the hydrogel surface which was in contact with the hydrophobic glass slide. All chemicals were purchased from Sigma Aldrich, USA.

To render the glass surface hydrophobic, glass slides (25 mm x 75 mm) were first rinsed liberally with dichlorodimethylsilane. The solution was left on the slide for 1 minute, before rinsing copiously with DI water, followed by subsequent drying. Coverslips were made hydrophilic to ensure the grafting of the hydrogels to their surface. Here, the coverslips were cleaned by UV-O₃ and then covered with a film of 0.1 M NaOH solution, which was allowed to evaporate evenly from the surface. Next, the coverslips were covered with 200 μL of 3-aminopropyltriethoxysilane (APTES) for 5 minutes, and then rinsed with DI water. Finally, the coverslips were immersed in a 0.5% (v/v) solution of glutaraldehyde in phosphate-buffered saline solution for half an hour with the NaOH and APTES treated surface facing up. Following a final rinse with DI water, the coverslips were ready to be used. All chemicals were obtained from Sigma Aldrich, USA.

2.2 Dynamic Light Scattering (DLS)

To prepare hydrogel samples for Dynamic Light Scattering (DLS), 750 µl of solution was pipetted into a microcuvette and allowed to gel for 1 day. DLS measurements were carried out in

triplicate samples and at least six measurements per sample. A particle analyzer (Zetasizer 3000, Malvern, USA) was used to conduct light scattering measurements on hydrogels at a fixed wavelength λ of 632 nm and a scattering angle θ of 90°. Single exponential decay functions were fit to the autocorrelation function based on Tanaka's model:³³

$$g^2(t) - 1 = A \cdot \exp(-\Gamma \cdot \tau)$$

Eq. (4)

Γ being the characteristic decay rate and A the amplitude of the relaxation mode. The decay rate is due to the cooperative diffusion of the polymer network, $D_c = \Gamma/Q^2$, with $Q = 4\pi n/\lambda \sin \theta/2$, and n=1.379, the refractive index of the solution. The correlation length responsible for this relaxation mode is calculated as $\xi = k_B T/(6\pi \eta D_c)$, where k_B is the Boltzmann constant, T the temperature, and η the solvent viscosity (~0.89 mPas at 25°C). It is widely recognized that the correlation length provides the mesh size of the polymer network of physically and chemically crosslinked hydrogels. Here, it is used to characterize the *bulk* microstructure of the three hydrogels.

2.3 Colloidal Probe Atomic Force Microscopy (AFM). An Atomic Force Microscope (Nano Wizard, JPK Instruments, Germany) was used for lateral force measurements and colloidal probe AFM indentation. All measurements were conducted with SiO₂ (silica) colloids of nominal radius equal to 10 μm (Duke Scientific, Thermo Scientific, USA). The colloids were attached to the end of tipless cantilevers (CSC37-No Al/tipless, Mikromash, nominal spring constant = 0.4 N/m) with an epoxy glue (JB-Weld, Sulphur Springs, TX, USA). Using a clean test grating (MikroMasch, Spain), reverse imaging of the attached colloids was conducted to determine the RMS roughness and it was found to be less than 5 nm over an area of 1 μm x 1μm. Before starting the experiments, the tips were rinsed in an ethanol bath and cleaned by UV-O₃ (Bioforce Nanoscience, Chicago,

IL) for half an hour. The normal stiffness of the cantilevers was determined by the thermal noise and the lateral calibration was performed following the modified Sader's method.³⁶

Lateral force measurements were conducted at various lateral velocities of the piezo (V) and loads (L) on all three hydrogels to determine static friction at room temperature. At the point of reversal of the piezo (i.e. under zero tangential force), the normal load was maintained constant for a period of time (t_{hold}) that ranged from 0 to 60 seconds; this was repeated three times per loading condition and sample. Normal loads between 2 and 50 nN were selected for the static friction-force measurements. The lateral velocity of the piezo was varied between 0.2 and 10 µm/s, while the scan length was kept constant at 28 µm. The minimum load was selected to be 2 nN (average pressure of 0.03, 0.044 and 0.062 kPa for 4%, 6% and 9% hydrogels, respectively), because static friction vanished at this load, perhaps due to the presence of a fluid film between the two surfaces.³⁷ The maximum load was limited to 50 nN to limit the contact radius (Table S1). The range of velocities was limited by the velocity at which contact ageing vanished at room temperature (0.2 µm/s). For temperature-dependent experiments, a petri dish heater (JPK Instruments, Germany) was used to modulate the temperature in the range of 25 to 60 °C. At least 3 hours of equilibration time were allowed at each selected temperature to ensure that hydrogels, sample holder, fluid, as well as colloid, were in thermal equilibrium. The temperature-dependent lateral force measurements were performed at varying normal loads and hold times, as described above, and constant lateral velocity of 1 µm/s, three times per loading condition and sample; loads higher than 30 nN were not applied in static friction measurements on 4% hydrogels above room temperature. Note that the number of measurements was limited to three per condition and sample in order to keep the duration of a single experiment below 20 hours. However, both temperaturedependent and room temperature measurements were repeated at least on three different samples of each hydrogel type on different days.

A GUI developed in MATLAB was used to read the value of the static friction. Both height and lateral deflection of the cantilever were inspected to ensure that pill-up did not happen. The static friction F_s was defined as the maximum lateral force before sliding started, which led to the drop of the friction force to the dynamic value. The average magnitude of the static friction and the standard deviation, which is shown as error bar in the diagrams, were calculated for each condition.

Indentation measurements were performed on each hydrogel sample at an approach/retraction velocity of 2 μ m/s at room temperature just before the friction measurements. The colloid was retracted after a hold time varying between 0 and 60 s, and the pull-off force (F_{adh}) was defined as the minimum value in the retraction curve; at least eight measurements were carried out per loading condition and sample in an area of 10 μ m x 10 μ m. An "effective" adhesion energy was obtained from the integral of the negative portion of the force-indentation depth curve upon retraction (see Figure S1a in the SI); the term "effective" indicates that the adhesion energy calculated from dynamic force measurements is not an equilibrium property. Pull-off force and effective adhesion energy correlate very well under all conditions, and hence, we show only the pull-off force in the manuscript. On selected samples (at least two per hydrogel type), the indentation measurements were carried out at modulated temperature between 25 °C and 50 °C.

2.4 Indentation model. The Johnson-Kendall-Roberts (JKR) model 38 was fit to the indentation force-depth curves upon retraction to determine the elastic modulus, the contact radius and the interfacial energy. The retraction curve was fit from the maximum indentation depth to the minimum force, i.e. the pull-off force (F_{adh} in Figure S1b). Following equations were used for the fits:

$$h = h_0 + \frac{a^2}{3R} + \frac{F}{2aE^*}$$

Eq. (1)

$$a^{3} = \frac{3R}{4E^{*}} \left(F + 3\pi\gamma R + (6\pi\gamma RF + (3\pi\gamma R)^{2})^{\frac{1}{2}} \right)$$

Eq. (2)

where F is the indentation force, h the indentation depth, h_o the contact point, R the colloid radius, a the contact radius, γ the interfacial energy, and E^* the contact elastic modulus defined as

$$\frac{1}{E^*} = \left(\frac{1 - v_{gel}^2}{E_{gel}}\right) + \left(\frac{1 - v_{sil}^2}{E_{sil}}\right)$$

Eq. (3)

 E_{gel} being the elastic modulus of the hydrogel, E_{sil} the elastic modulus of the silica colloid (72.2 GPa ³⁹), and ν the Poisson's ratio of the hydrogel ($\nu_{gel}=0.45$) and silica colloid ($\nu_{sil}=0.168$), respectively. Three fitting parameters (h_0 , E^* and γ) were determined from the fit of Eqns. 1-3 to the experimental data νia a least squared curve fitting algorithm built in MATLAB.

In addition to this, the Hertz model⁴⁰ ($F = \frac{4}{3}E^*R^{1/2}h^{3/2}$) was used to fit the indentation forcedepth curves upon extension of the colloid to the hydrogel "piecewise". As recently reported by Spencer's group,⁴¹ this method enables to estimate the change of the elastic modulus as a function of indentation depth, and thereby, to characterize the graded microstructure of the hydrogels from the surface into the bulk.

3. RESULTS

3.1 Correlation length of the polymer network

The influence of the hydrogel's composition on the correlation length of the polymer network was investigated by DLS. Figure S2 shows representative DLS results for the three hydrogels. A

single-exponential function was fit to determine the fast decay corresponding to the collective diffusion of the polymer network. The plateau at longer decay times results likely from inhomogeneities.⁴² However, the magnitude is too small to be fit by a second exponential decay.⁴³ Stretched exponentials did not improve the fits to the experimental data, neither.

The (de Gennes') correlation length corresponding to the fast decay (ξ) is 9.9±0.4, 8.2±0.6 and 7.1±0.8 nm for 4%, 6% and 9% PAAm hydrogels, respectively. This correlation length represents the distance between crosslinks in a hydrogel, and hence, it is a measure of the mesh size. These values agree well with the reported mesh size obtained by small angle x-ray scattering for PAAm hydrogels (9.4±1.1 nm and 7.0±0.5 nm for 3.8 and 7.5 wt.% hydrogels).⁴⁴

3.2 Room temperature static friction and adhesion

AFM lateral force measurements were conducted with a silica colloid glued to the end of a tipless cantilever (Figure 1a). A constant normal load (L) was applied on the hydrogel for a period of time (static loading time or hold time, t_{hold}) before the cantilever was pulled laterally at constant velocity (V) by a piezo. Figure 1b illustrates the lateral force after selected hold times as a function of the piezo position in representative measurements. The static friction (F_s) is defined as the maximum lateral force before sliding commences, which is characterized by the sudden drop in friction to the value given by the dynamic friction (F_d). Figures 1c-e show the static friction (average values and standard deviation) as a function of hold time at the selected normal loads of 5, 10, 30 and 50 nN for c) 4%, d) 6% and e) 9% hydrogels, respectively. The JKR average pressure is in the range 0.03-0.2, 0.55-0.91, 0.15-1.03 kPa for 4%, 6% and 9% hydrogels, respectively; see the maximum pressure in Table S1. For each specific loading time, the measured static friction increases with normal load in a sublinear fashion, as illustrated in Figure S3 in the SI. A sublinear relation was also reported for the dynamic friction vs. normal load of these hydrogels, 32 and the

deviation from Amonton's law (i.e. the linear relation between friction and load) was attributed to the significant increase in adhesion with applied load.

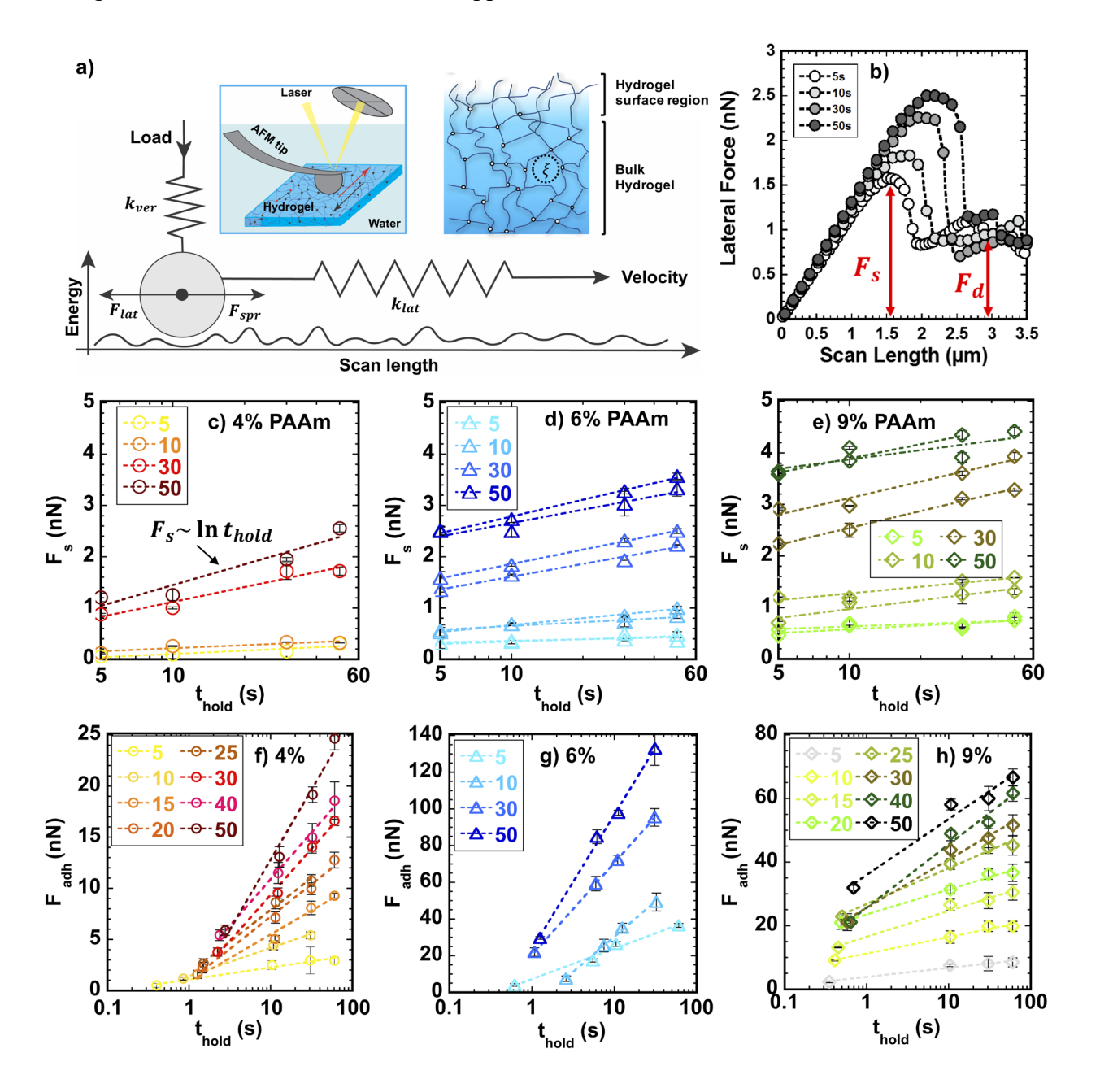


Figure 1. a) Schematics of lateral force measurements by AFM. When the colloid is laterally pulled, it experiences a lateral force F_{lat} , which leads to a torsion of the cantilever, while the applied load (L) is maintained constant. The laser reflected by the cantilever quantifies its deflection, and the lateral force is determined with the lateral spring constants (k_{lat}) . b) Lateral

force measured while the cantilever is laterally pulled at a velocity (V) of 2 µm/s after loading times (t_{hold}) of 5, 10, 30 and 60 s (L=50 nN) for a 6 % hydrogel. The diagram shows static friction (F_s) and dynamic friction (F_d); c-e) Static friction vs. hold time at normal loads of 5, 10, 30 and 50 nN for c) 4% (circles in red-yellow shades), d) 6% (triangles in blue shades) and e) 9% (diamonds in green shades) hydrogels, at lateral velocities of 5 µm/s (dash-dotted line) and 10 µm/s (dashed line). The lines represent logarithmic fits ($F_s \sim \ln t_{hold}$) with R²-values better than 0.85 at loads larger than 5 nN (see Table S1); the fits exhibit occasionally smaller R²-values under 5 nN. f-h) Pull-off force (F_{adh}) vs. hold time (t_{hold}) at normal loads between 5 and 50 nN (see legend) for f) 4%, g) 6% and h) 9% hydrogels at an approach/retraction velocity of 2 µm/s; the hold time includes the contact time during extension of the colloid, which is smaller than 2.5 s in all cases. In all diagrams in this work, the markers give the average and the error bars represent the standard deviation. Colloid radius = 10.6 µm. Cantilever stiffness= 0.42 N/m.

The static friction increases with the hold time for the three hydrogels (Figures 1c-e). Note that the static friction at zero hold time, not shown on the logarithmic x-axis, is insignificant; representative measurements are shown in Figure S4. The static friction also varies with the lateral velocity (V), as illustrated in Figures 1d-e for 5 and 10 μ m/s (dash-dotted and dashed lines, respectively). Figure 2 provides additional evidence for the change in static friction with lateral velocity for the three hydrogels. While at the lowest velocities the influence is not evident, the static friction increases with velocity above 0.5 μ m/s. These results demonstrate that the time under shear loading before sliding occurs (i.e. while the piezo moves at the selected velocity V and the lateral force increases to F_s) affects the magnitude of the static friction. We hypothesize that, while the cantilever is pulled (after point of time 0 in Figure 1b), the viscoelastic relaxation of the

polymer network dissipates part of the energy stored upon static loading, which reduces the static friction. Less prominent relaxation can happen at faster velocities, which justifies the increase in static friction.

The increase of static friction with hold time at room temperature in Figures 1c-e is reminiscent of the contact ageing characteristic of dry interfaces that was described in the Introduction. The relation is close-to-logarithmic at room temperature, with R^2 values larger than 0.85 at loads above 5 nN in the range of lateral velocities from 0.5 to 10 μ m/s (see Table S2). However, an exponential function, which points at a saturation of the contact area with time, yields sometimes similar R^2 -values. Hence, the ageing relation for the static friction cannot be unambiguously determined in the narrow range of investigated hold times. For simplification, we refer to it as *quasi* logarithmic. Further, the static friction clearly deviates from a logarithmic increase with hold time at room temperature at the slowest probed velocity of 0.2 μ m/s; see e.g. Figure 2 at 30 nN. Here, the static friction appears to remain constant or even decrease with hold time. As described later, this behavior is close to the *thermodynamic limit*. ⁴⁵ While we report the limiting behavior at 0.2 μ m/s, this work targets the behavior at velocities between 0.5 and 10 μ m/s.

The pull-off force (F_{adh}) was measured upon retraction of the colloid from the hydrogels after hold times varying between 0 and 50 s (Figure 1f-h). Similar to the static friction of the three hydrogels at room temperature, the pull-off force increases with the logarithm of the loading time for the three hydrogels (Figure 1f-h). This supports that the increase in static friction with hold time is associated to the adhesion of the hydrogel to the colloid, which is consistent with the *adhesion model* described in the Introduction and often applied to explain static friction at dry interfaces. ¹⁶ The highest pull-off forces were measured for 6% hydrogels, while the smallest values

were obtained for 4% hydrogels. This can be explained by the contribution of both the interfacial energy (γ) and the contact area (A_r) to adhesion, as follows. Using the JKR model ³⁸ to analyze the indentation force-depth curves upon retraction, both terms, γ (0.08±0.03, 0.32±0.08, 0.55±0.15 mN/m for 4%, 6% and 9% hydrogels, respectively) and A_r (see Table S1 in the SI) were determined. Although the interfacial energy is highest for 9% hydrogels, perhaps stemming from their largest polymer concentration, the contact area between 6% hydrogels and the colloid is larger than that of 9% hydrogels (with smaller mesh size and greater elastic modulus), which justifies the greater pull-off force on 6% hydrogels. While the contact area between the colloid and 4% hydrogels is the largest, the interfacial energy (γ) is about one order of magnitude smaller, which leads to the smallest values of the pull-off force.

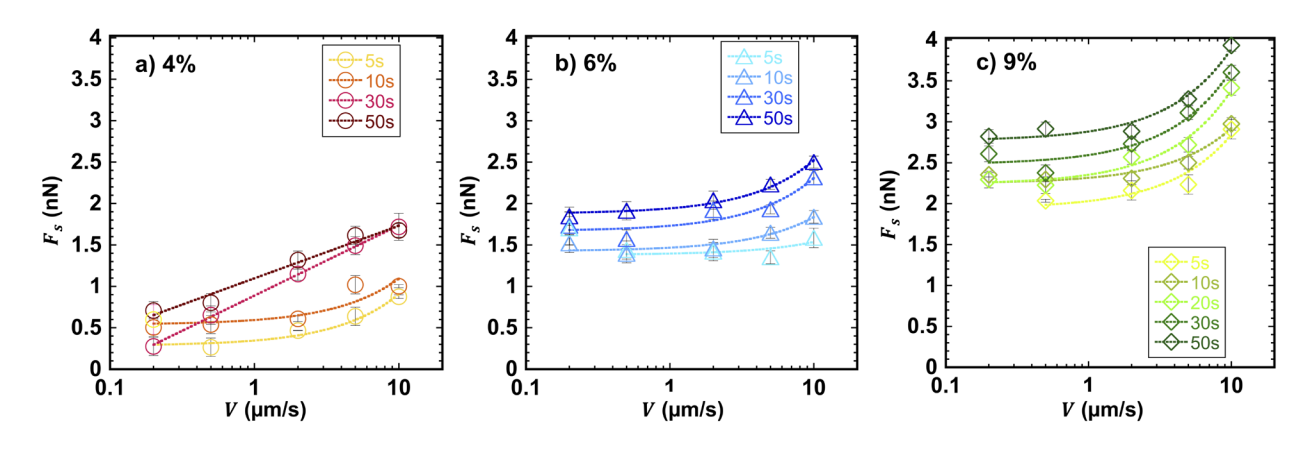


Figure 2. Static friction (F_s) as a function of the lateral velocity (V) for a) 4%, b) 6% and c) 9% hydrogels at different hold times t_{hold} (see legend, in seconds) upon an applied load of 30 nN. Colloid radius = 10.6 μ m. Cantilever stiffness = 0.42 N/m. The lines are to guide the eye.

3.3 Temperature-dependence of static friction and adhesion

Pull-off and lateral force measurements were also conducted as a function of temperature ranging between 25 and 60 °C. Representative results of the static friction as a function of temperature are shown in Figure 3 for 6% and 9% hydrogels. The prominent variation of the static friction with temperature reveals a local minimum and either one or two local maxima in the static friction, which are labeled as T_{min} , T_p and T_p^* , respectively. The higher shade intensity represents longer hold times before pulling the cantilever laterally. Overall, the most prominent increase in static friction with hold time is observed for 6% hydrogels. While the variation in static friction with an increment of t_{hold} by 5 seconds is often small, the temperature-induced change of the relation between static friction and hold times is statistically significant. This is more evident in Figure 4. Here, the dashed lines represent the fits to a logarithmic function of the hold time. Deviations from a logarithmic trend are generally observed when the temperature increases above room temperature. For instance, an increase of temperature to 50°C results in a reversed change of the static friction with hold time at 20 nN (Figure 4a), while a *quasi* logarithmic trend is preserved up to an applied load of ~50 nN (Figure 4b). For 9% hydrogels, in contrast, the static friction already decreases with hold time at temperatures above 30°C at the same load (Figure 4d). In fact, the reverse trend, i.e. a decrease of static friction with longer hold times, is more pronounced on 9% hydrogels above 30 – 40 °C. Finally, the static friction of 4% hydrogels decreases slightly with temperature and achieves a plateau above 30°C (Figure 5), while it only increases with hold time at 25°C and 30°C (Figure 4c). It is thus evident that the microstructure of the hydrogels plays an important role in dictating the relation between static friction, temperature and hold time.

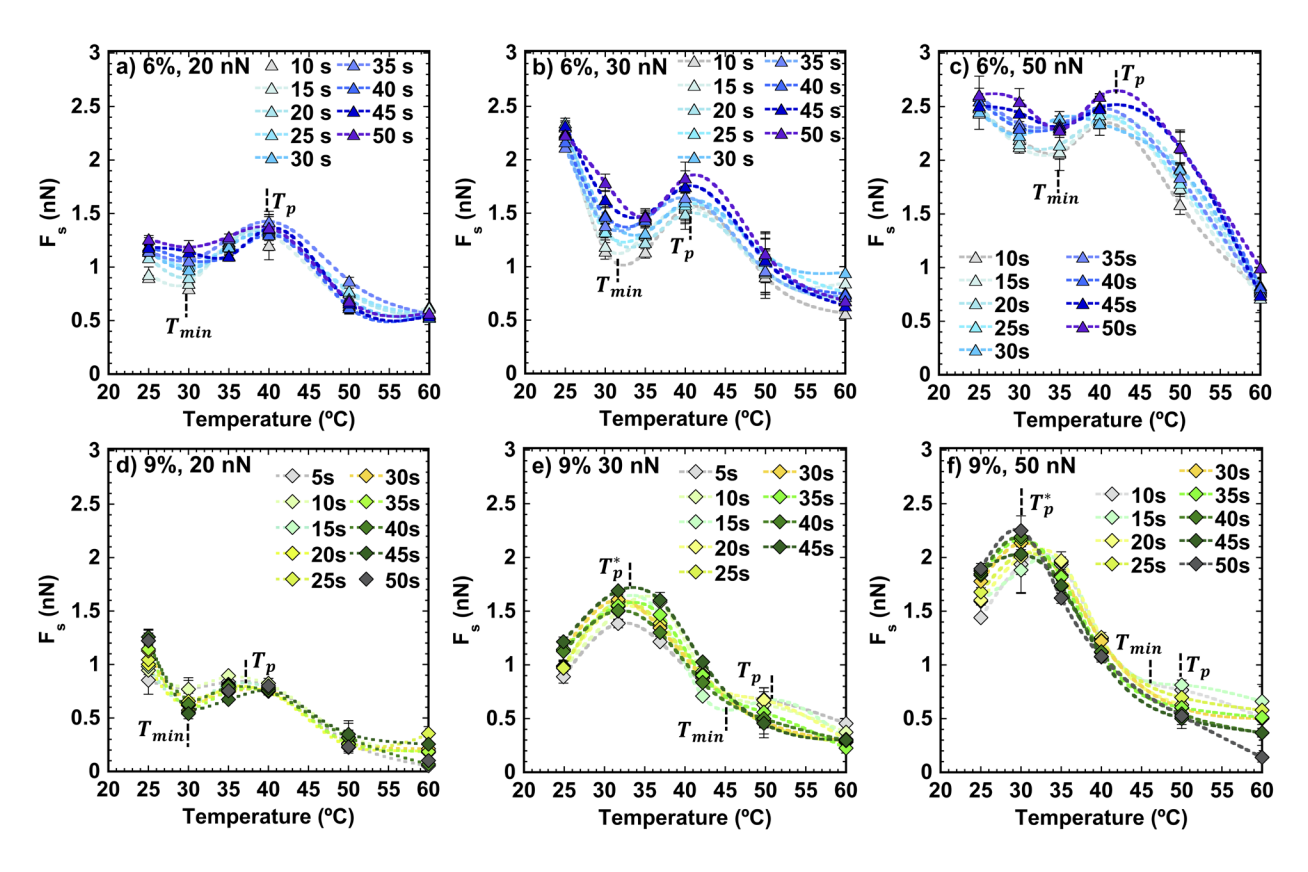


Figure 3. Static friction F_s as a function of temperature for different hold times between 5 s and 50 s (see legends) for 6% hydrogels at a) 20, b) 30 and c) 50 nN, and for 9% hydrogels at d) 20, e) 30 and f) 50 nN. The lines show the fits of the experimental results to spline functions to estimate T_p^* , T_p and T_{min} ; a collection of the characteristic temperatures is shown in Figure 8b. Colloid radius = 10.7 μ m. Cantilever stiffness= 0.42 N/m. Lateral velocity: 1 μ m/s.

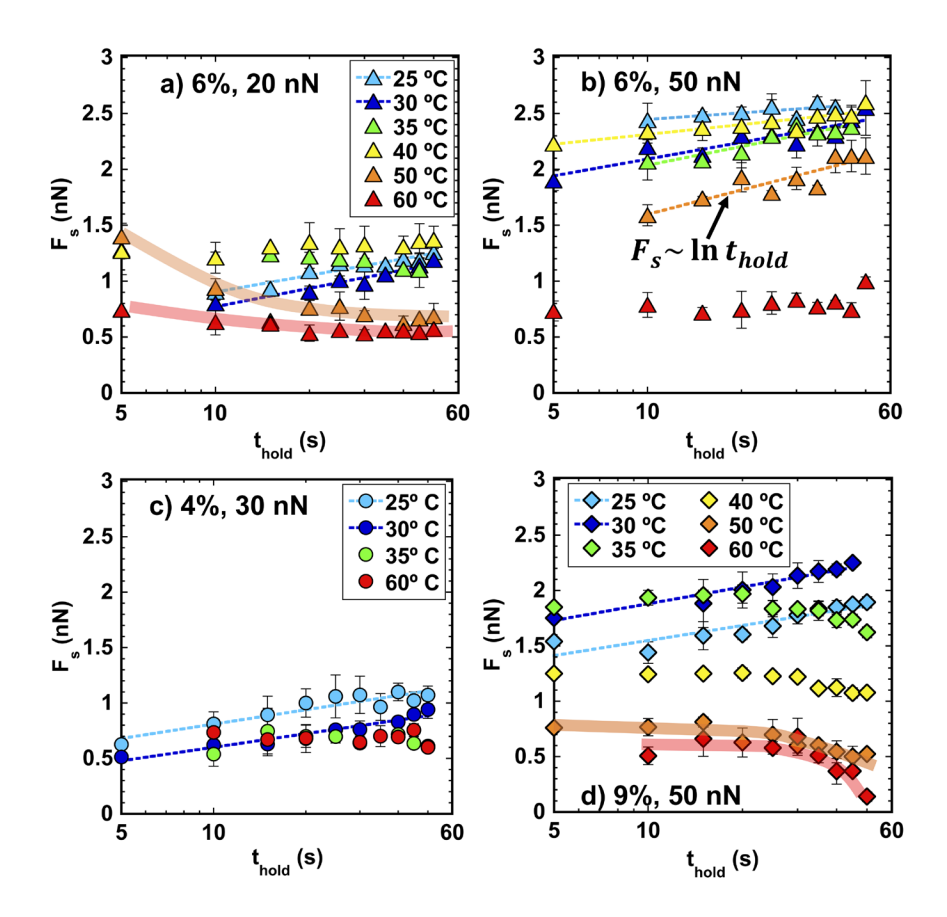


Figure 4. Static friction F_s as a function of hold time t_{hold} measured at 25 °C (light blue), 30 °C (dark blue), 35 °C (green), 40 °C (yellow), 50 °C (orange) and 60 °C (red) for 6% hydrogels at (a) 20 and (b) 50 nN, (c) 4% hydrogels at 30 nN and (d) 9% hydrogels at 50 nN. The dashed lines represent a logarithmic fit to the data, with a regression coefficient R^2 better than 0.87. The thick semi-transparent lines are to guide the eye. Colloid radius = 10.7 μm. Cantilever stiffness = 0.42 N/m. Lateral velocity: 1 μm/s.

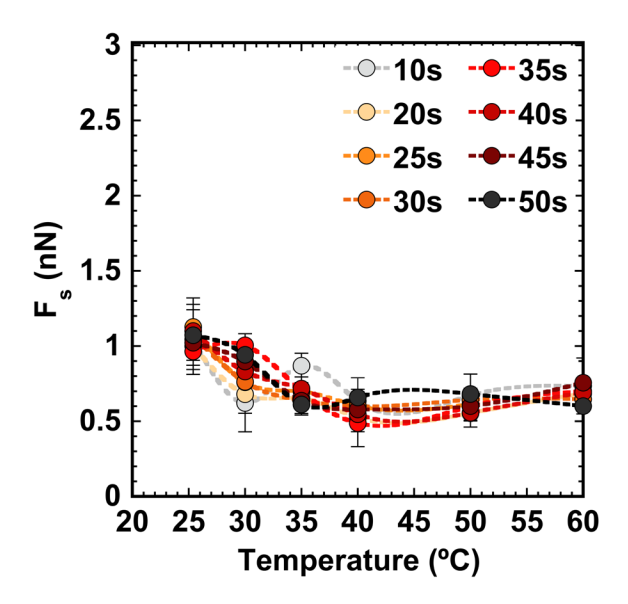


Figure 5. Static friction F_s as a function of temperature for different hold times between 5 s and 50 s for 4% hydrogels at 30 nN. Colloid radius = 10.7 μ m. Cantilever stiffness= 0.42 N/m. Lateral velocity: 1 μ m/s.

Similarly, the change of the pull-off force with temperature is non-monotonic and strongly dependent on hydrogel's composition (Figure 6). The pull-off force between the silica colloid and 4% hydrogels drops initially with temperature, and then, it plateaus, qualitatively similar to the change in static friction shown in Figure 5. A prominent decrease in pull-off force with increase in temperature and the highest values in pull-off force are observed for 6% hydrogels; local minima and maxima (θ_{min} and θ_p , in analogy to T_{min} and T_p) are obvious at loads smaller than 40 nN. Note that this hydrogel exhibits the highest static friction above room temperature and most prominent contact ageing. In the case of 12% hydrogels, the pull-off force also varies non-monotonically with temperature, with very prominent extrema (θ_p^* , in analogy to T_p^*) under all applied loads. These results support that (non-monotonic) changes in adhesion with temperature may underlie the variation in static friction, as discussed later.

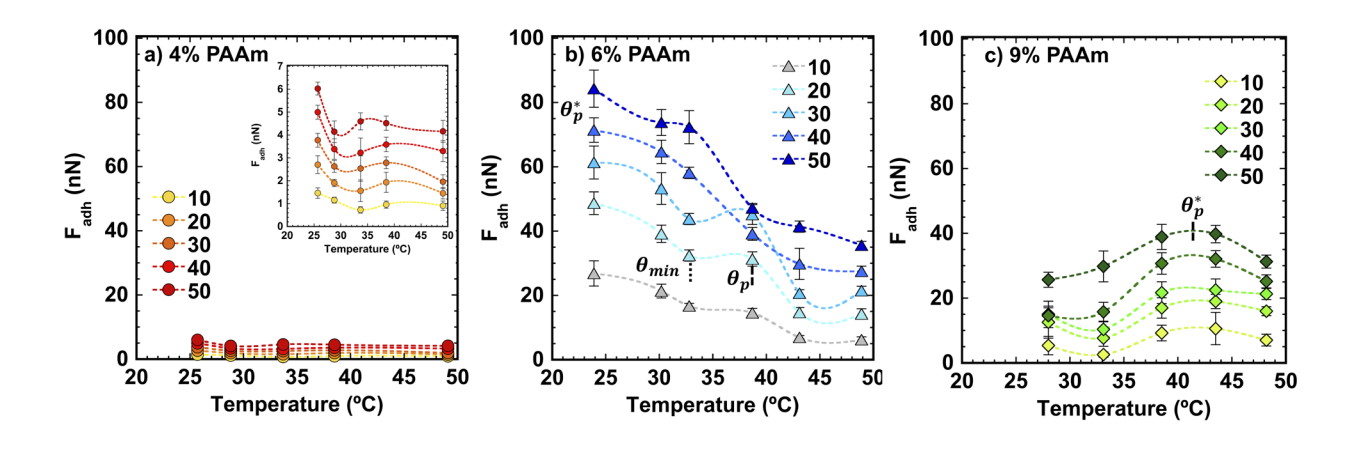


Figure 6. Pull-off force (F_{adh}) as a function of temperature for a) 4% PAAm, b) 6% PAAm and c) 9% PAAm hydrogels. The applied normal load prior to the retraction of the cantilever was varied between 10 and 50 nN (see legend). The inset in a) shows a magnification of the pull-off force. The contact times (before retraction) range from 0.8, 0.5, and 0.2 s (at the load of 10 nN) to 2.4, 1.2, and 0.8 (at the load of 50 nN) for 4, 6 and 9% PAAm hydrogels, respectively. The lines show the fits of spline functions. Extension and retraction speed = 1 μm/s. Colloid radius = 10.7 μm. Cantilever stiffness = 0.42 N/m.

3.3 Elastic moduli from indentation experiments

The elastic moduli were determined using the JKR model to fit the indentation force-depth curves upon retraction. Figure 7 shows the elastic moduli of 4%, 6% and 9% hydrogels as a function of the temperature. In the case of 9% hydrogels, the elastic modulus decreases by 45% as the temperature increases from 25.4 to 48.2 °C upon an applied normal load of 10 nN, while at higher loads (20 – 50 nN) the decrease of the modulus with increase in temperature ranges from 4 to 8 %. Similarly, a decrease in modulus is also seen for 6% hydrogels when the temperature is increased, but the influence of the temperature appears to be less significant under high loads. Because the viscosity of water decreases with an increase in temperature, a faster drainage is

expected at higher temperatures, and thereby, a larger contact area. If the change in the pull-off force with temperature would solely result from a change of contact area, an inverse correlation between the elastic modulus (E) and the pull-off force would be expected ($i.e.\ F_{adh} \sim A_r \sim E^{-2/3}$). The comparison of Figures 6 and 7 provides evidence for the lack of such correlation.

Figure 7c also reveals that (i) the elastic moduli measured under an applied load of 10 nN are significantly smaller than at higher loads; (ii) at 40 and 50 nN, the influence of load on the modulus is not statistically significant; (iii) and the behavior is transitional at 20 and 30 nN. We attribute these results to the well-known inhomogeneous polymerization of polyacrylamide hydrogels close to a hydrophobic surface, which leads to reduced crosslinking near the surface. 46 A recent study of the graded mechanical response of 7.5% PAAm hydrogels has shown that the less dense and crosslinked (brush-like) surface layer can be as thick as 2 µm.41 To examine the graded microstructure of the PAAm hydrogels, the Hertz model was fit piecewise to the indentation forcedepth curves upon extension of the colloid (Figure S5). This practice yields a surface layer of 640 \pm 75 nm, 330 \pm 200 and 250 \pm 92 nm for 4%, 6% and 9% hydrogels, respectively, with an elastic modulus of only $\sim 335 \pm 120$, 455 ± 139 , and 482 ± 176 Pa. The elastic modulus increases gradually with depth and a modulus equal to 1.05 ± 0.08 , 8.7 ± 0.4 , and 16.5 ± 3.8 kPa is achieved at depths of 640 \pm 75 nm, 620 \pm 92 nm and 467 \pm 27 nm for 4%, 6% and 9% hydrogels, respectively, which does not vary further with depth. Hence, the smaller elastic moduli determined at 10 nN compared to measurements at higher loads may originate from the more significant influence of the hydrogel's surface region with reduced crosslinking at smaller indentation depths. This effect appears less prominent for 4% and 6% hydrogels compared to 9% hydrogels (note the smaller difference between the elastic moduli determined at the different loads), which seems reasonable considering the smaller difference between the elastic moduli of these hydrogels'

surface region and bulk. The non-uniform thickness of this skin may justify the large standard deviation of the elastic modulus.

Based on this, we propose that this brush-like "skin" has a thickness in the range of hundreds of nanometers. Interestingly, a softening of the surface of 6% and 9% hydrogels (probed at 10 nN) is reproducibly observed at 50 °C, the highest examined temperature. We associate this to the increased fluctuation rate of the near-surface dangling polymer chains at high temperature.⁴⁷ The higher crosslinking of the sub-surface hydrogel (probed at higher loads) makes the elastic modulus less susceptible to changes in temperature.

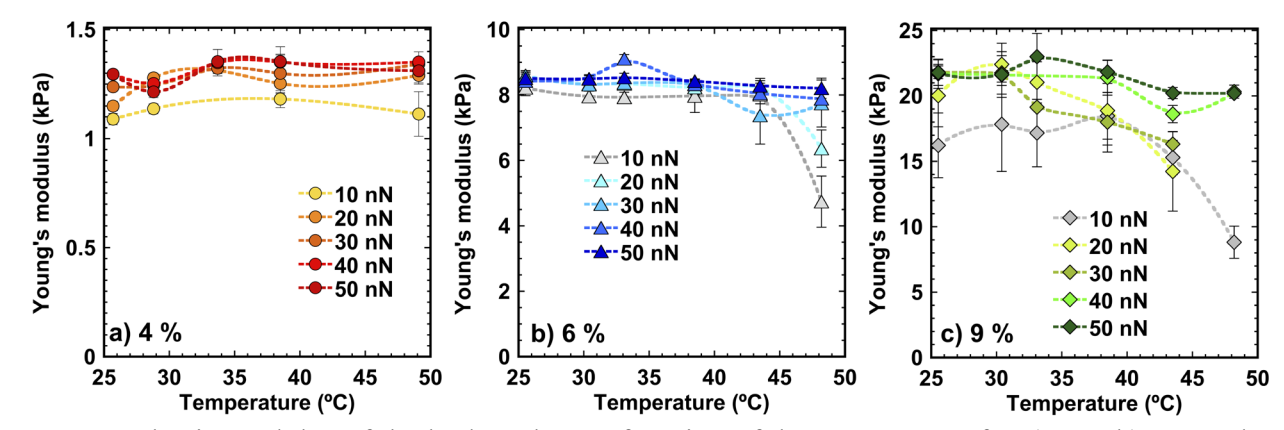


Figure 7. Elastic modulus of the hydrogels as a function of the temperature for a) 4%, b) 6% and c) 9% hydrogels. The same data are shown in Figure S6 with the load in the X-axis and the temperature in the legend. Colloid radius = $10.7 \mu m$. Cantilever stiffness = 0.42 N/m. Extension and retract speed: $1 \mu m/s$.

4. DISCUSSION

The change of hydrogel's static friction with temperature is non-monotonic (Figure 3). Friction of rubbers has been reported to peak at a characteristic temperature and velocity.⁴⁸ This was reconciled by Israelachvili in a phase diagram for adhesion hysteresis and friction as a function of the Deborah number, $D_e = \tau/t$ (τ being a characteristic relaxation time and t the observation

time).⁴⁵ The Deborah number characterizes the material fluidity, i.e. the observation that, given enough time, even a solid will flow. At large Deborah numbers (low temperature, short observation time, high velocity), there is not sufficient time for the polymer to relax, so that it behaves like a solid. If there is enough time for relaxation to happen (high temperature, long time, slow velocity), the polymer network behaves liquid-like. The influence of the temperature on static friction can be described *via* a rate process of polymer attachment to and detachment from the colloid that determines the number of adhesive bonds and their average life time. Being thermally activated, both rates are promoted by an increase in temperature. If the interfacial polymer's behavior is solid-like, an increase in temperature enhances the number of adhesive bonds, and thereby, adhesion and static friction. In case of liquid-like behavior, the mobility of the polymer increases with temperature, which promotes detachment of the polymer from the colloid, and thereby, it decreases the average life of the adhesive bonds. This would yield a decrease in adhesion and friction with increase in temperature and justify a peak in static friction.

This picture can be applied to hydrogels, as well. The rates of attachment (detachment) of flexible polymers like polyacrylamide to (from) the colloid are related to the reptation time in the context of the scaling theory, $\tau_P^0 \sim \eta \xi^3/k_B T$, η being the viscosity of water, k_B the Boltzmann constant, T the temperature, and ξ , the mesh size.³⁴ Since the adhesion to the colloid is an interfacial phenomenon, the relevant relaxation time is that of the (brush-like) superficial layer, whose thickness (ξ_s) was estimated in indentation experiments. Assuming a brush length between ~ 0.65 to 0.35 µm (i.e. the correlation length of the brush), the relaxation time τ_P^0 would be ~ 0.01 - 0.08 s; while τ_P^0 for the bulk mesh size is smaller than ~ 0.2 µs at room temperature. The applied pressure leads to squeeze-out of water and to an increase in polymer concentration within the stressed region, which further restricts the mobility of the interfacial polymer in a concentrated

solution, while confined by the colloid. Accordingly, the relaxation time at the confined interface (τ_P) is expected to be greater than τ_P^0 . For example, it increases by ~two orders of magnitude upon confinement of polymer melts.⁴⁹ In static friction measurements, the observation time is inversely proportional to the lateral velocity, $t \sim \xi_S/V$. Under the conditions of our experiments, t ranges between 0.04 and 3.3 s, and hence, it is expected to be close to τ_P , which implies that the effects of the viscoelastic relaxation can be examined in our experiments.

Viscoelastic polymer relaxation would lead to a single peak in the static friction as a function of temperature, as described above. The change in hydrogel's static friction with temperature is, however, more intricate, and a local minimum at T_{min} is reproducibly observed, which announces the existence of two maxima, T_p and T_p^* . Importantly, a second peak was measured in dynamic friction of rubbers against rough surfaces and attributed to the ploughing or deformation of the rubber surface as the track asperities passed over it.⁴⁸ Note that this may be relevant upon sliding, but not when the material is subjected to shear loading before sliding happens, like here. As biphasic polymeric materials holding large amounts of water, hydrogels undergo also poroelastic relaxation, which is related to the pressure-induced drainage of the interstitial water.⁵⁰ Taking into account that the osmotic modulus of the relaxed hydrogels is close to the shear storage modulus (G') determined under volume conserving conditions in rheological measurements⁵¹ $(G' \sim 143, 275)$ and 1141 Pa for our hydrogels, from ref. ³¹), the applied pressure (Table S1) overcomes the osmotic modulus under most of the loading conditions. Pressures above the osmotic modulus cause a redistribution of water and polymer within the stressed region.⁵²

The relevance of this phenomenon in our experiments is supported by the estimated poroelastic relaxation times $\tau_W = 6\pi\eta a^2/P\xi^2$, a being the contact radius and P the pressure.⁵⁰ To estimate the mesh size that limits the poroelastic relaxation, the indentation depths were determined on the

indentation force-depth curves as a function of load; see summary in Figure S7. With increase in load, the indentation depth becomes larger than the "skin" of the hydrogels, which suggests that the drainage rate is limited by the bulk mesh size ($\xi \sim 9.9 \pm 0.4$, 8.2 ± 0.6 and 7.1 ± 0.8 nm). This yields values of τ_W between 5 and 45 s, i.e. in the range of the selected hold times (Figure S8). Furthermore, the decrease in viscosity of the interstitial water with temperature (from 0.89 mPa.s at 25°C to 0.60 mPa.s at 50°C) should lead to a greater drainage rate, and thereby, contact area, which would contribute to the increase in static friction with temperature. In fact, an increase of temperature from 25 to 50°C leads to an increase in indentation depth by 322 ± 40 , 375 ± 43 and 113 ± 19 nm for 4%, 6% and 9% hydrogels, respectively. This supports the relevance of the poroelastic relaxation in dictating the change of contact area with temperature in our experiments.

Based on this, it is proposed that the superposed poroelastic and polymer relaxation associated to the biphasic nature of hydrogels dictate the change of the static friction with temperature, which is generalized in a phase diagram in Figure 8a (black line). At temperatures below T_p^* , the static friction increases with an increase of temperature, which is associated with the solid-like response of the (compressed) hydrogel's interfacial region; here, polymer attachment to the colloid is enhanced with temperature, yielding an increase in the shear strength of the interface (σ_s) according to the adhesion model. The peak at lower temperature (T_p^*) is, however, only obvious in the case of 9% hydrogels (Figure 3d-f), the hydrogel with the highest polymer concentration and the thinnest surface layer, which suggests that the investigated temperatures are too high to probe this behavior in 4 and 6 % hydrogels, with thicker and softer surface layers and looser networks underneath. In the range of examined temperatures, the decrease in static friction with temperature is most prominent. This reflects the liquid-like behavior of the polymer above T_p^* , i.e. the decrease in life time of the adhesive bonds with temperature, which justifies the decrease of shear strength

 σ_s , and thereby, of static friction. Hence, T_p^* represents an "interfacial" glass transition temperature, as also recognized for the dynamic friction of rubbers; interestingly, Grosch found the interfacial glass transition to occur at ~50 K above the bulk glass transition. ⁴⁸ Concurrently, the contact area A_r increases with temperature during static loading, as justified above. This partially compensates the decrease in shear strength due to the liquid-like behavior of the polymer network. These two competing mechanisms are at the root of the more or less pronounced extrema at T_p and T_{min} . Above T_p , the liquid-like behavior of the interfacial polymer dictates the decrease of the static friction with temperature.

 T_{min} and T_P were estimated for 6% and 9% hydrogels by fitting a spline function to the results in Figures 3a-f and the values are depicted in Figure 8b. A spline function is a piecewise polynomial function, whose extrema can be found by derivation of a continuous function. It is evident that T_{min} and T_P shift to higher temperatures with polymer concentration (Figure 8c), consistent with the results for T_p^* . In the case of 4% hydrogels, T_{min} and T_P were not measured above 25°C. Note that the range of investigated temperatures is limited in our AFM, and therefore, we only probe a small region of the phase diagram. Here, the behavior of 4% hydrogels seems to achieve the so-called "bulk thermodynamic limit" (dashed line), where the hydrogel has enough time to reach a fully relaxed state, and the influence of the temperature vanishes.⁴⁵

Importantly, when higher loads are applied, opposite trends are expected from both contributions: the viscoelastic relaxation time (τ_P) should increase due to the enhanced polymer concentration (as more water is squeezed out) and the induced restriction of mobility upon confinement; while the poroelastic time (τ_W) decreases with load, leading to a faster growth of the contact area (Figure S8). The former should promote the solid-like behavior of the hydrogel and shift the phase diagram to higher temperatures, 45 while the later should decrease the temperature

at which T_{min} is achieved. When the load is increased from 20 to 30 nN, the shift of T_{min} and T_p (for 6% and 9% hydrogels, Figure 8b) and of T_p^* (for 9% hydrogels) to higher temperatures suggests that the viscoelastic relaxation time dictates the influence of the load on the hydrogel's static friction. The influence of load on the static friction phase diagram is thus schematically shown in Figure 8d. On the other hand, upon a further increase of load to 50 nN, T_p and T_{min} remain approximately constant, and hence, it is possible that the effect of the poroelastic relaxation starts to become more significant at sufficiently high pressures.

Per temperature-time superposition principle, ⁴⁵ the same conceptual phase diagram justifies the influence of the lateral velocity ($V \sim t^{-1}$) on static friction. As shown in Figure 2, static friction was shown to increase with velocity above 0.5 µm/s at room temperature, while the trend was unclear at slower velocities. This is likely because the liquid-like behavior of the hydrogels is mainly probed at room temperature if V>0.5 µm/s (observation time $t < \xi_s(\mu m)/0.5$), while at slower velocities, i.e. at longer observation times, the behavior becomes closer to the thermodynamic limit.

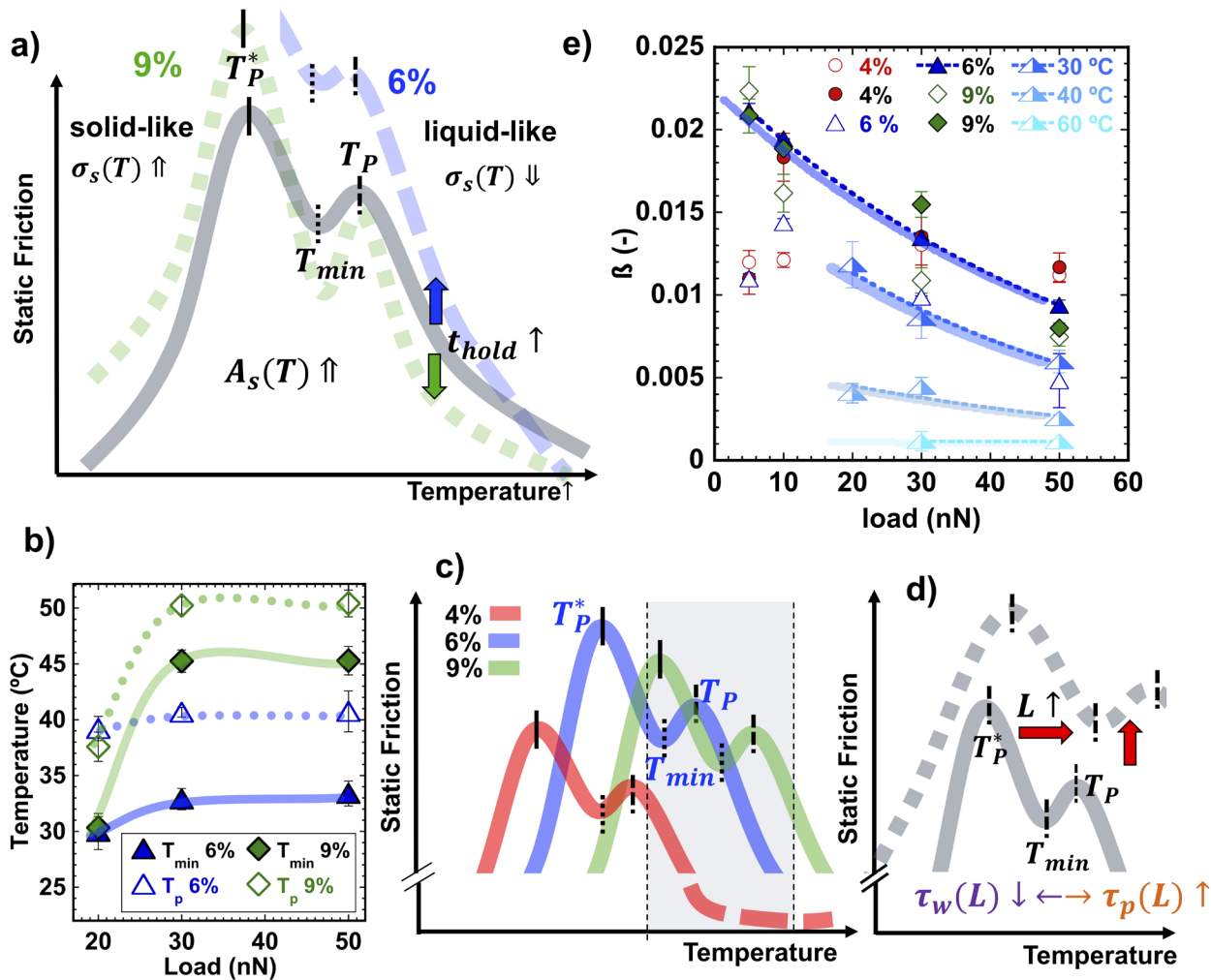


Figure 8. a) Phase diagram of hydrogels' static friction and effect of the increase in hold time. Per analogy to the dynamic friction phase diagram of rubbers, the X-axis could also be the lateral velocity, from large to small values. The characteristic temperatures T_{min} and T_p shift to higher values with decrease in mesh size and are shown in b) as average and standard deviation in the range of investigated hold times. T_{min} and T_p for 9% hydrogels at 30 and 50 nN correspond only to $t_{hold} < 20$ s, because they vanish at longer loading times. Schematic effects of c) hydrogel's composition and d) load on the static friction phase diagram. e) Logarithmic slope β_s^L at selected velocities of 10 μ m/s (full markers) and 2 μ m/s (empty markers) for the three hydrogels at 25°C and only for 6% hydrogels at higher temperatures (30 °C, 40 °C, 60 °C, split triangles).

Both the effective adhesion energy and the pull-off force follow a non-monotonic trend as a function of temperature. Note that an adhesion hysteresis phase diagram has been proposed before for dry interfaces. 45 Adhesion hysteresis is the difference between the work needed to separate two surfaces and that originally gained on bringing them together. In the case of hydrogels, the hydration-polymer mediated repulsion is negligible compared to the significant adhesion to the colloid upon separation, and hence, adhesion hysteresis and adhesion are believed to be roughly analogous for hydrogels. The results in Figures 6 can be explained based on the same model; that is, the concomitant effects of poroelastic and polymer relaxation of hydrogels give rise to two peaks $(\theta_p$ and $\theta_p^*)$ and a local minimum (θ_{min}) in the adhesive force. Considering the large error bars in the results of 4% hydrogels and the small adhesion, we believe that θ_p is smaller than room temperature in this case, and a state close to the bulk thermodynamic limit is probed, as for the static friction. In the case of 6% hydrogels, it is possible that θ_p^* is close to 25°C. However, the measurements should be extended to lower temperatures to unambiguously determine θ_p^* . Nevertheless, the smaller magnitude of θ_p^* (\lesssim 25°C) for 6% compared to 9% hydrogels (~40-43°C) is consistent with the results for the static friction. A difference between static friction and adhesion phase diagrams is that θ_{min} and θ_p of 6% hydrogels vanish at high loads. This might be partially originated by the much shorter hold (loading) times applied in temperature-dependent pull-off force experiments (<2.4 s) compared to static friction measurements (5-50 s), which mitigates the influence of the poroelastic relaxation. Another difference is that θ_{min} and θ_{p} are not detected for 9% hydrogels and θ_p^* is ~ 42°C, i.e. much higher than T_p^* (~30-33°C). We cannot exclude that the different results partially originate from the distinct loading conditions in adhesion and static

friction force measurements (e.g. the latter ones are under shear loading) but this requires further investigation.

The increase in static friction with the time of static loading (t_{hold}) is a characteristic of the investigated hydrogel-silica interfaces at sufficiently high lateral velocity close to room temperature. A logarithmic relation is also observed for the pull-off force vs. loading time, supporting that the mechanism underlying contact ageing is related to an increase in adhesion with the duration of static loading, as proposed by adhesion models. To quantify contact ageing, the empiric expression, $F_s = L(\alpha_s^L + \beta_s^L \ln t_{hold})$ (from ref.)¹⁶ was fit to the experimental results exhibiting a logarithmic relationship with reasonable R²-values (>0.85); the corresponding logarithmic slopes (β_s^L) are shown in Figure 8e. The slope is of the same order of magnitude for the three hydrogels, which suggests that, despite the differences in the hydrogels' composition, the underlying mechanisms are similar. The higher values of β_s^L at 10 $\mu m/s$ compared to 2 $\mu m/s$ reflect that the viscoelastic relaxation upon slow shear (before sliding commences) attenuates the ageing rate. While β_S^L is of the same order of magnitude than that reported for polymer glasses far from their glass transition, 16 i.e. small, our results are intrinsically different. First, β_s^L for polymer glasses increases by a factor of ~3-4 around their glass transition because the polymer mobility increases. In contrast, the logarithmic increase of the static friction with hold time is lost on 4% and 9% hydrogels above ~30-40°C and the decrease in β_s^L with increase in temperature in the case of 6% hydrogels indicates that the ageing rate also becomes less severe. Second, the increase in load leads to a prominent decrease in β_s^L , which indicates that the ageing rate becomes progressively alleviated. This might reflect the faster saturation of the contact area with increase in load.

Considering that both relaxation times are of relevance under the investigated conditions, it is proposed that the superposed effects of polymer relaxation at the confined interface and of fluid drainage also dictate the change of static friction with loading time; the former affects the timedependent interfacial strength $\sigma_s(t_{hold})$ and the latter influences the true contact area $A_r(t_{hold})$. This lets us reconcile our results with the adhesion model, which gives the static friction as $F_s(t_{hold}) = A_r(t_{hold}) \cdot \sigma_s(t_{hold})^{16}$ The key differences from previous works are that the change of σ_s of the hydrogels with time is non-monotonic; and that drainage of the interstitial water leads to a monotonic increase of A_r with hold time that might saturate at high load. The result is an intricate evolution of hydrogel's static friction with hold time that gradually deviates from the classical logarithmic relationship when the temperature increases (Figure 8a, dashed lines). Hence, contact ageing of the glass-hydrogel interface happens at $T < T_p^*$ due to both the poroelastic and the polymer relaxation. Above T_p^* , the liquid-like behavior of the polymer increasingly mitigates contact ageing due to the promoted polymer detachment from the colloid. Here, the increase of static friction with hold time is dictated by the fluid drainage and the corresponding increase in contact area. Beyond T_p , the prominent decrease of the static friction of 9% hydrogels with hold time is the signature of the dominating liquid-like behavior of this interface. Interestingly, at sufficiently high temperature, this behavior leads to similar values of the static friction of 9% and 4% hydrogels, despite the different polymer (and water concentrations). This implies that higher water contents do not necessarily yield lower static friction coefficients; in contrast to the findings for hydrogel's dynamic friction of Gemini interfaces at room temperature.⁵³ Further, the growth of the contact area (and of adhesion) with time is more prominent for 6% compared to 9% hydrogels, which promotes the increase in static friction with time up to higher temperatures in 6% hydrogels.

The findings of this work help understand previous studies of hydrogel friction, which reported a non-monotonic dependence of the *dynamic* friction between hydrogels on the sliding velocity. A generalized Tabor expression can be also used for the dynamic friction, $F_d = \sigma_s(V) \cdot A_r(\phi)$, ϕ being the age of the contact. The dynamic friction of 6% hydrogels was observed to decrease with sliding velocity, whereas the opposite was measured for 9% hydrogels in the same range of velocities. This can be attributed to the more significant ageing of the 6% hydrogels-silica interface compared to 9% hydrogels. That is, longer contact times of the migrating contact area yield a greater A_r , which justifies the increase in dynamic friction with slower sliding velocity. In contrast, the increase in dynamic friction of the 9% hydrogels is consistent with the dominant influence of the interfacial strength and its solid-like behavior.

The proposed phase diagram provides a new understanding of static friction, which should be universal for hydrogel-like materials, like those ubiquitous in biological tribosystems. The experimental results demonstrate the intricate role of both the hydrogel's (bulk) mesh size and the near-surface region, characterized in this work by different correlation lengths. This helps understand better the role of stratified microstructures of biological tribosystems with low-density surface layers holding large amounts of water, like the superficial gel-like layer on articular cartilage. Interestingly, our ongoing research indicates that the superficial zone of bovine cartilage exhibits static frictional characteristics similar to 9% PAAm hydrogels.

Optimal design of advanced hydrogel-based materials for cartilage replacement should afford control of strength, toughness and lubricious properties, as well as enhance cell growth. Single-network hydrogels are good candidates due to their hydrophilicity and biocompatibility, yet they pose vital limitations related to their mechanical integrity. Hence, interpenetrating double network (DN) hydrogels have emerged as promising replacement candidates due to their high

strength and toughness, yet often at the cost of higher friction.⁵⁷⁻⁵⁸ For instance, a recent study on DN hydrogels showed that, underneath a "hard" surface layer, the remaining hydrogel provided low friction coefficient, but it was much softer, 58 emphasizing the challenge to afford control of both hydrogel's toughness and interfacial forces by design. The knowledge emerging from this work supports that hydrogels with graded microstructures that combine a tough hydrogel with a brush-like low-dense surface region can reduce the increase in static friction with loading time, and thereby wear, if properly designed (cf. 4%, 6% and 9% hydrogels). Interestingly, it has been shown that adding a third *non-crosslinked* polymer to a double network hydrogel can yield a very low friction coefficient.⁵⁷ Together with the results of our work, this supports alternative design strategies based on covalently grafting a flexible non-crosslinked polymer to the surface of a strong and tough DN hydrogel as well as stratified gelation. Nevertheless, open questions that remain to be addressed in future include the influence of functional groups with different chemical composition and charge, composition of the (bio)lubricant, as well as of the semiflexibility of the macromolecules, characteristics that could affect the frictional response. We believe that the implications of this work go beyond biolubrication and biomedical applications and extend to soft robotics and micro-electromechanical devices, where the processes occurring at the migrating hydrogel interface are of relevance.

Conclusions

Hydrogels are central to biological lubrication, but little is known about the origin of their malfunctions and how to prevent them. Here, colloidal probe AFM was used to investigate the static friction between a silica colloid and polyacrylamide hydrogels as a function of load, loading time, sliding velocity and temperature. Despite the enormous amounts of water held in hydrogels,

our results support that adhesion to the silica surface is responsible for the change in static friction with temperature, which is observed to greatly depend on the hydrogel composition. This work has revealed two main mechanisms underlying static friction, namely the polymer viscoelasticity within the confined interfacial region and the poroelastic relaxation due to fluid drainage. The experimental results demonstrate the intricate role of both the hydrogel's (bulk) mesh size and the composition of the near-surface region, characterized by different correlation lengths, in dictating static friction and how it can be modulated by varying temperature, loading time and pressure (load). Based on these phenomena, a static friction phase diagram that accounts for the biphasic nature of hydrogels has been proposed. The present work supports that modulating the hydrogel's mesh size and its surface region is a means to control static friction, contact ageing, and thereby, wear of hydrogel-like materials. The fundamental knowledge derived from this work provides insight about biolubrication and guidance for the design of functional gels.

ASSOCIATED CONTENT

Supporting Information. The following file is available free of charge on the ACS Publications website at DOI: XXX.

The Supporting Information contains figures with representative indentation curves and fit using the JKR model, correlation functions obtained from DLS, friction loops under zero loading time, static friction as a function of normal loads, elastic modulus as a function of normal load at multiple temperatures, piecewise Hertz fits to indentation force curves, indentation depths as a function of load, estimated poroelastic relaxation times as a function of normal load and adhesion energy as a function of temperature. It also includes a table with the regression coefficients of the logarithmic

fits to static friction vs. hold time, and a table with contact radii and contact pressures in the preformed experiments.

AUTHOR INFORMATION

Corresponding Author

* Rosa M. Espinosa-Marzal (rosae@illinois.edu)

Author Contributions

The manuscript was written through contributions of all authors. All authors have given approval to the final version of the manuscript.

ACKNOWLEDGMENT

This work is supported by the National Science Foundation Grant No. 17-61696. We thank Prof.

N. D. Spencer, Dr. R. Simic and Prof. Mark Robbins for fruitful discussions.

REFERENCES

- 1. Jin, Z.; Dowson, D., Bio-friction. *Friction* **2013**, *I* (2), 100-113.
- 2. Guilak, F., Compression-induced changes in the shape and volume of the chondrocyte nucleus. *J Biomech* **1995**, *28* (12), 1529-41.
- 3. Guilak, F.; Ratcliffe, A.; Mow, V. C., Chondrocyte deformation and local tissue strain in articular cartilage: a confocal microscopy study. *J Orthop Res* **1995**, *13* (3), 410-21.
- 4. Moore, A. C.; Burris, D. L., Tribological rehydration of cartilage and its potential role in preserving joint health. *Osteoarthritis Cartilage* **2017**, *25* (1), 99-107.
- 5. Ateshian, G. A., The role of interstitial fluid pressurization in articular cartilage lubrication. *Journal of biomechanics* **2009**, *42* (9), 1163-1176.
- 6. Crockett, R., Boundary Lubrication in Natural Articular Joints. *Tribol Lett* **2009**, *35* (2), 77-84.
- 7. Crockett, R.; Roos, S.; Rossbach, P.; Dora, C.; Born, W.; Troxler, H., Imaging of the surface of human and bovine articular cartilage with ESEM and AFM. *Tribol Lett* **2005**, *19* (4), 311-317.
- 8. Crockett, R.; Grubelnik, A.; Roos, S.; Dora, C.; Born, W.; Troxler, H., Biochemical composition of the superficial layer of articular cartilage. *J Biomed Mater Res A* **2007**, *82* (4), 958-64.

- 9. Kumar, P.; Oka, M.; Toguchida, J.; Kobayashi, M.; Uchida, E.; Nakamura, T.; Tanaka, K., Role of uppermost superficial surface layer of articular cartilage in the lubrication mechanism of joints. *J Anat* **2001**, *199* (Pt 3), 241-50.
- 10. Sawae, Y.; Murakami, T.; Matsumoto, K.; Horimoto, M., Study on morphology and lubrication of articular cartilage surface with atomic force microscopy. *J Jpn Soc Tribologis* **2000**, *45* (2), 150-157.
- 11. Bell, C. J.; Ingham, E.; Fisher, J., Influence of hyaluronic acid on the time-dependent friction response of articular cartilage under different conditions. *Proc Inst Mech Eng H* **2006**, 220 (1), 23-31.
- 12. Forster, H.; Fisher, J., The influence of loading time and lubricant on the friction of articular cartilage. *Proc Inst Mech Eng H* **1996**, *210* (2), 109-19.
- 13. Nitzan, D. W., 'Friction and adhesive forces'--possible underlying causes for temporomandibular joint internal derangement. *Cells Tissues Organs* **2003**, *174* (1-2), 6-16.
- 14. Lee, D. W.; Banquy, X.; Israelachvili, J. N., Stick-slip friction and wear of articular joints. *Proc Natl Acad Sci U S A* **2013**, *110* (7), E567-74.
- 15. Beddoes, C. M.; Whitehouse, M. R.; Briscoe, W. H.; Su, B., Hydrogels as a Replacement Material for Damaged Articular Hyaline Cartilage. *Materials (Basel)* **2016**, *9* (6), 443.
- 16. Berthoud, P.; Baumberger, T.; G'Sell, C.; Hiver, J. M., Physical analysis of the state- and rate-dependent friction law: Static friction. *Phys Rev B* **1999**, *59* (22), 14313-14327.
- 17. Mazo, J. J.; Dietzel, D.; Schirmeisen, A.; Vilhena, J. G.; Gnecco, E., Time Strengthening of Crystal Nanocontacts. *Phys Rev Lett* **2017**, *118* (24), 246101.
- 18. Lorenz, B.; Krick, B. A.; Rodriguez, N.; Sawyer, W. G.; Mangiagalli, P.; Persson, B. N., Static or breakloose friction for lubricated contacts: the role of surface roughness and dewetting. *J Phys Condens Matter* **2013**, *25* (44), 445013.
- 19. Ben-David, O.; Rubinstein, S. M.; Fineberg, J., Slip-stick and the evolution of frictional strength. *Nature* **2010**, *463* (7277), 76-9.
- 20. Gong, J. P., Friction and lubrication of hydrogels—its richness and complexity. *Soft Matter* **2006**, *2* (7), 544-552.
- 21. Peppas, N. A., *Hydrogels in medicine and pharmacy: properties and applications*. CRC PressI Llc: Boca Raton, Florida, 1987; Vol. 3.
- 22. Kwon, H. J.; Yasuda, K.; Gong, J. P.; Ohmiya, Y., Polyelectrolyte hydrogels for replacement and regeneration of biological tissues. *Macromol Res* **2014**, *22* (3), 227-235.
- 23. Spiller, K. L.; Maher, S. A.; Lowman, A. M., Hydrogels for the repair of articular cartilage defects. *Tissue Eng Part B Rev* **2011**, *17* (4), 281-99.
- 24. Datta, S. S.; Preska Steinberg, A.; Ismagilov, R. F., Polymers in the gut compress the colonic mucus hydrogel. *Proc Natl Acad Sci U S A* **2016**, *113* (26), 7041-6.
- 25. Juvekar, V. A.; Singh, A. K., Rate and Aging Time Dependent Static Friction of a Soft and Hard Solid Interface. *arXiv print* **2016**, *Cornell University*.
- 26. Baumberger, T.; Caroli, C.; Ronsin, O., Self-healing slip pulses and the friction of gelatin gels. *Eur Phys J E Soft Matter* **2003**, *11* (1), 85-93.
- 27. Nitta, T.; Kato, H.; Haga, H.; Nemoto, K.; Kawabata, K., Static Friction of Agar Gels: Formation of Contact Junctions at Frictional Interface. *J Phy Soc Jpn* **2005**, *74* (11), 2875-2879.
- 28. Kagata, G.; Gong, J. P.; Osada, Y., Friction of Gels. 7. Observation of Static Friction between Like-Charged Gels. *J Phys Chem B* **2003**, *107* (37), 10221-10225.
- 29. Suzuki, A.; Ishii, R.; Yamakami, Y.; Nakano, K., Surface friction of thermoresponsive poly(N-isopropylacrylamide) gels in water. *Colloid Polym Sci* **2011**, *289*, 561-568.

- 30. Drury, J. L.; Mooney, D. J., Hydrogels for tissue engineering: scaffold design variables and applications. *Biomaterials* **2003**, *24* (24), 4337-4351.
- 31. Shoaib, T.; Espinosa-Marzal, R. M., Insight into the Viscous and Adhesive Contributions to Hydrogel Friction. *Tribol Lett* **2018**, *66* (3), 96.
- 32. Shoaib, T.; Heintz, J.; Lopez-Berganza, J. A.; Muro-Barrios, R.; Egner, S. A.; Espinosa-Marzal, R. M., Stick-Slip Friction Reveals Hydrogel Lubrication Mechanisms. *Langmuir* **2018**, *34* (3), 756-765.
- 33. Tanaka, T.; Hocker, L. O.; Benedek, G. B., Spectrum of light scattered from a viscoelastic gel. *J Chem Phys* **1973**, *59* (9), 5151-5159.
- 34. de Gennes, P. G., *Scaling Concepts in Polymer Physics*. Cornell University Press: New York, 1991.
- 35. Hwang, J. S.; Cummins, H. Z., Dynamic light scattering studies of gelatin gels. *J Chem Phys* **1983**, 79 (10), 5188-5193.
- 36. Cannara, R. J.; Eglin, M.; Carpick, R. W., Lateral force calibration in atomic force microscopy: A new lateral force calibration method and general guidelines for optimization. *Rev Sci Instrum* **2006**, *77* (5), 053701.
- 37. Grest, G. S.; Murat, M., Structure of grafted polymeric brushes in solvents of varying quality: a molecular dynamics study. *Macromolecules* **1993**, *26* (12), 3108-3117.
- 38. Johnson, K. L.; Kendall, K.; Roberts, A. D., Surface energy and the contact of elastic solids. *Proc. R. Soc. Lond. A* 324, 301-313.
- 39. Pabst, W.; Gregorova, E., Elastic Properties of Silica Polymorphs a Review. *Ceram-Silikaty* **2013**, *57* (3), 167-184.
- 40. Hertz, H., Über die Berührung fester elastischer Körper. *Reine Angewandte Mathematik* **1881,** *92*, 156-171.
- 41. Meier, Y. A.; Zhang, K.; Spencer, N. D.; Simic, R., Linking Friction and Surface Properties of Hydrogels Molded Against Materials of Different Surface Energies. *Langmuir* **2019**.
- 42. Shibayama, M.; Norisuye, T., Gel Formation Analyses by Dynamic Light Scattering. *B Chem Soc Jpn* **2002**, *75* (4), 641-659.
- 43. Herning, T.; Djabourov, M.; Leblond, J.; Takerkart, G., Conformation of gelatin chains in aqueous solutions: 2. A quasi-elastic light scattering study. *Polymer* **1991**, *32* (17), 3211-3217.
- 44. Urueña, J. M.; Pitenis, A. A.; Nixon, R. M.; Schulze, K. D.; Angelini, T. E.; Sawyer, G. W., Mesh Size Control of Polymer Fluctuation Lubrication in Gemini Hydrogels. *Biotribology* **2015**, *1-2*, 24-29.
- 45. Israelachvili, J. N., *Intermolecular and surface forces*. 3rd ed.; Academic press: 2011.
- 46. Kii, A.; Xu, J.; Gong, J. P.; Osada, Y.; Zhang, X., Heterogeneous Polymerization of Hydrogels on Hydrophobic Substrate. *J Phys Chem B* **2001**, *105* (20), 4565-4571.
- 47. Klein, J., The Interdiffusion of Polymers. *Science* **1990**, *250* (4981), 640-646.
- 48. Grosch, K. A., The relation between the friction and visco-elastic properties of rubber. *P Roy Soc A-Math Phys* **1963**, *274* (1356), 21-39.
- 49. Peanasky, J.; Cai, L. L.; Granick, S.; Kessel, C. R., Nanorheology of Confined Polymer Melts. 3. Weakly Adsorbing Surfaces. *Langmuir* **1994**, *10* (10), 3874-3879.
- 50. Sokoloff, J. B., Theory of hydrostatic lubrication for two like-charge polymer hydrogel coated surfaces. *Soft Matter* **2010**, *6* (16), 3856-3862.
- 51. Geissler, E.; Hecht, A. M.; Horkay, F.; Zrinyi, M., Compressional modulus of swollen polyacrylamide networks. *Macromolecules* **1988**, *21* (8), 2594-2599.

- 52. Schulze, K. D.; Hart, S. M.; Marshall, S. L.; O'Bryan, C. S.; Urueña, J. M.; Pitenis, A. A.; Sawyer, W. G.; Angelini, T. E., Polymer Osmotic Pressure in Hydrogel Contact Mechanics. *Biotribology* **2017**, *11*, 3-7.
- 53. Pitenis, A. A.; Sawyer, W. G., Lubricity of High Water Content Aqueous Gels. *Tribol Lett* **2018**, *66* (3), 113.
- 54. Baumberger, T.; Berthoud, P.; Caroli, C., Physical analysis of the state- and rate-dependent friction law. II. Dynamic friction. *Phys Rev B* **1999**, *60* (6), 3928-3939.
- 55. Means, A. K.; Shrode, C. S.; Whitney, L. V.; Ehrhardt, D. A.; Grunlan, M. A., Double Network Hydrogels that Mimic the Modulus, Strength, and Lubricity of Cartilage. *Biomacromolecules* **2019**, *20* (5), 2034-2042.
- 56. Vega, S. L.; Kwon, M. Y.; Burdick, J. A., Recent advances in hydrogels for cartilage tissue engineering. *Eur Cell Mater* **2017**, *33*, 59-75.
- 57. Kaneko, D.; Tada, T.; Kurokawa, T.; Gong, J. P.; Osada, Y., Mechanically strong hydrogels with ultra-low frictional coefficients. *Adv Mater* **2005**, *17* (5), 535-538.
- 58. Zhang, K.; Simic, R.; Yan, W.; Spencer, N. D., Creating an Interface: Rendering a Double-Network Hydrogel Lubricious via Spontaneous Delamination. *ACS Appl Mater Interfaces* **2019**, *11* (28), 25427-25435.